

Scattering times and mobility with localized impurities in topological insulator films

Parijat Sengupta* and Enrico Bellotti

Photonics Center

*Department of Electrical and Computer Engineering,
Boston University, Boston, MA 02215*

The zero gap surface states of a 3D-topological insulator host highly mobile Dirac fermions with spin locked to the momentum. The high mobility attributed to absence of back scattering is reduced in presence of impurities on the surface. In particular, we discuss and compare scattering times for localized impurities on the surface, scattering between states of opposite helicity located on different surfaces coupled through a hybridization potential, and the role of magnetic impurities. Magnetic impurities give rise to an additional spin suppression factor. The role of warped bands and its influence on topological factors that can enhance the overall surface mobility is examined.

I. Introduction

The zero gap helical surface states¹ of a 3D topological insulator (TI) film can be split by an external magnetic field or a reduction of film thickness.² Such a band gap open topological insulator loses protection against back scattering^{3,4} and has a reduced surface mobility. The suppression of mobility is also observed through large-angle scattering in presence of impurities on the surface of a TI with a consequent degradation of its charge transport properties. Further, a sufficiently thin film, with preserved time reversal symmetry, allows the possibility of a surface electron (a Dirac fermion) to back scatter⁵ by tunneling through the bulk and eventually occupy a state of opposite helicity on the bottom surface thus providing a pathway for velocity reduction. Inter and intra-band scattering events on the Dirac hyperbolas⁶ of each surface, created by splitting the TI states with an external magnetic field or a layered ferromagnet offers a way to probe phenomena such as weak anti-localization,^{7,8} electric conductivity, and localized magnetic moments through magnetoresistance measurements.

In this work, within a Boltzmann approximation, the impurity scattering time for surface carriers is evaluated (Sec. II) in a topological insulator film. The impurities are assumed to be non-interacting. Scattering times are evaluated for four cases 1) a zero-gap non-trivial topological insulator 2) in presence of inter-surface coupling 3) with substrate induced intrinsic dipole moments and 4) with a finite magnetic moment with an out-of-plane component that introduces a spin induced suppression factor. The corresponding semi-classical mobilities (Sec. III) derived from a linearized Boltzmann equation and a relaxation time approximation are discussed. The role of warping⁹ and its influence on overall transport behaviour is also highlighted. Results are collected in Sec. IV followed by concluding remarks.

II. Scattering rates for a localized impurity

Surface states in topological insulators such as Bi₂Te₃, Bi₂Se₃, and Sb₂Te₃ are characterized by a linear dispersion for small values of the momentum vector and a single Dirac cone at the Γ point. The calculations carried out in this work are partly performed using a low-energy

continuum four-band k.p Hamiltonian for 3D TIs. The four-band k.p Hamiltonian¹⁰ is further simplified in to a two-band Dirac Hamiltonian that represents only the linearly dispersing surface states; additional modifications that arise on account of higher warping terms are included later for comparison. The four-band k.p Hamiltonian in the basis set of the four lowest low-lying states $|P1_z^+ \uparrow\rangle$, $|P2_z^- \uparrow\rangle$, $|P1_z^+ \downarrow\rangle$, and $|P2_z^- \downarrow\rangle$ is

$$H(k) = \epsilon(k) + \begin{pmatrix} M(k) & A_1 k_z & 0 & A_2 k_- \\ A_1 k_z & -M(k) & A_2 k_- & 0 \\ 0 & A_2 k_+ & M(k) & -A_1 k_z \\ A_2 k_+ & 0 & -A_1 k_z & -M(k) \end{pmatrix} \quad (1)$$

where $\epsilon(k) = C + D_1 k_z^2 + D_2 k_\perp^2$, $M(k) = M_0 + B_1 k_z^2 + B_2 k_\perp^2$ and $k_\pm = k_x \pm ik_y$. For Bi₂Te₃ and Bi₂Se₃, the relevant parameters are taken from Ref. 11. The Hamiltonian is diagonalized numerically to obtain eigen values. The simplified two-dimensional Dirac Hamiltonian for the surface states can be written as¹¹

$$H_{surf.states} = \hbar v_f (\sigma_x k_y - \sigma_y k_x) \quad (2)$$

where v_f denotes *Fermi*-velocity and σ_i ; $i = x, y$ are the Pauli matrices. The corresponding density of states in standard notation is

$$D(\epsilon) = \int \frac{dk}{(2\pi)^2} \delta(\epsilon - E(k)) \quad (3a)$$

Changing to polar coordinates,

$$\begin{aligned} D(\epsilon) &= \frac{1}{(2\pi)^2} \int_0^{2\pi} d\theta \int_0^\infty k dk \frac{1}{\hbar v_f} \delta\left(k - \frac{\epsilon}{\hbar v_f}\right) \\ &= \frac{2}{2\pi (\hbar v_f)^2} |\epsilon| \end{aligned} \quad (3b)$$

The density of states of electrons described by the two-band Hamiltonian (Eq. 2) with spin degeneracy included is linear in energy and vanishes at the Dirac point. In deriving this expression, we have used the property $\delta(-x) = \delta(x)$.

This form of the Hamiltonian, though in principle sufficient to probe the surface states, fails to account for

the underlying crystal symmetries.¹²⁻¹⁴ A more accurate representation (Eq. 4) within the two-band model¹⁵ that is consistent with the C_{3v} point-group symmetry of the rhombohedral crystal, the snow-flake Fermi contour obtained from ARPES, and also preserves time reversal symmetry must contain higher order terms cubic in k . The next set of corrections involve k^5 terms¹⁶ which are ignored in all calculations here.

$$H(k) = \epsilon_0(k) + \hbar v_f (\sigma_x k_y - \sigma_y k_x) + \frac{\lambda}{2} \hbar^3 (k_+^3 + k_-^3) \sigma_z \quad (4)$$

$\epsilon_0(k)$ introduces the particle-hole anisotropy and the cubic terms denote warping. Using Eq. 4, and ignoring particle-hole anisotropy without loss of generality, the surface state spectrum is

$$\epsilon_{\pm}(k) = \pm \sqrt{\hbar v_f^2 k^2 + \lambda^2 \hbar^6 k^6 \cos^2(3\theta)} \quad (5)$$

where $\theta = \tan^{-1}(k_y/k_x)$.

The scattering rate on surface of a topological insulator due to localized and static non-magnetic impurity with a spherical potential $V = V_0 \delta(r - R_j)$ can be evaluated using the Fermi-Golden rule. The concentration of impurities is assumed to be dilute such that there are no interference effects between successive scattering events. The matrix element is

$$M(k', k) = \langle \Psi_f | V | \Psi_i \rangle \quad (6a)$$

where the two-component wave function Ψ for the linear Hamiltonian (Eq. 2) is

$$\Psi_{\eta} = \frac{1}{\sqrt{2}} \begin{pmatrix} \lambda_{\eta}(k) \exp(-i\theta) \\ \eta \lambda_{-\eta}(k) \end{pmatrix} \quad (6b)$$

and

$$\lambda_{\eta}(k) = \sqrt{1 \pm \frac{\Delta}{\sqrt{\Delta^2 + (\hbar v_f k)^2}}} \quad (6c)$$

A. Scattering rate between states of identical helicity

The helicity of the electron wave function is denoted by $\eta = \pm$ and Δ represents a band gap for the surface states. Evaluating the square of the matrix element for a ungapped TI film when an electron elastically scatters through an angle ϕ between states with identical helicity gives

$$|M(k', k)|^2 = |\langle \Psi_f | V_0 | \Psi_i \rangle|^2 = V_0^2 \cos^2 \frac{\phi}{2} \quad (7)$$

and $\phi = \theta_f - \theta_i$. The elastic scattering time using a Boltzmann approximation^{17,18} such that $|k| = |k'|$ is

$$\frac{1}{\tau} = \frac{2\pi}{\hbar} \int \frac{d^3 k'}{8\pi^3} \delta(\epsilon_k - \epsilon_{k'}) |\chi_{kk'}| (1 - \cos\phi) \quad (8)$$

where $\chi_{kk'} = |M(k', k)|^2 \zeta(s, s')$. The additional spin-scattering factor $\zeta(s, s')$ takes in to account the helical spin structure of the TI surface states. For a pristine TI, $\zeta(s, s') = \cos^2 \frac{\phi}{2}$ with $0 \leq \phi \leq \pi$, since back scattering is forbidden and the factor must assume a value between zero and unity. The integral in Eq. 8 therefore must be integrated over all values of ϕ .

$$\begin{aligned} \frac{1}{\tau} &= \frac{2\pi}{\hbar} g(\epsilon) \int_0^{\pi} V_0^2 \cos^4 \frac{\phi}{2} (1 - \cos\phi) d\phi \\ &= \frac{\pi \epsilon}{\hbar^3 v_f^2} \frac{V_0^2}{4} \end{aligned} \quad (9)$$

where we have used Eq. 3b for density of states $g(\epsilon)$. The impurities on the surface can also be of several types, each with a different density, which means that Eq. 9 must be modified to reflect this situation

$$\frac{1}{\tau} = \sum_{n_i} \frac{2\pi}{\hbar} g(\epsilon) \int_0^{\pi} n_i V_{0i}^2 \cos^4 \frac{\phi}{2} (1 - \cos\phi) d\phi \quad (10)$$

where n_i and V_{0i} denote a particular impurity density and the related scattering potential.

B. Scattering rate between opposite surfaces

The two opposite surfaces in a topological insulator host states of opposite helicity; therefore, for the possibility of scattering to happen between two such states, the topological insulator film must be sufficiently thin. A thin film TI can be modeled as

$$H_{surf.states} = \hbar v_f (\sigma_x k_y - \sigma_y k_x) + \Delta_h \sigma_z \quad (11)$$

where $2\Delta_h$ is the band gap shift. The scattering rate can be similarly computed by employing the Fermi-golden rule, the square of the matrix element now is given as $V_0^2 \sin^2 \frac{\phi}{2}$. Inserting the expression for matrix element in Eq. 8, we get

$$\begin{aligned} \frac{1}{\tau} &= \frac{2\pi}{\hbar} g(\epsilon) \frac{V_0^2 (\hbar v_f k)^2}{\Delta^2 + (\hbar v_f k)^2} \int_0^{\pi} \sin^2 \frac{\phi}{2} \cos^2 \frac{\phi}{2} (1 - \cos\phi) d\phi \\ &= \frac{\pi \epsilon}{4\hbar^3 v_f^2} \frac{V_0^2 (\hbar v_f k)^2}{\Delta^2 + (\hbar v_f k)^2} \end{aligned} \quad (12)$$

Topological insulator thin films are usually grown on substrates that render the structure asymmetric by adding an intrinsic dipole moment and breaking structural inversion symmetry (SIA). Such a thin film with an inherent SIA potential U can be described by the Hamiltonian

$$H_{surf.states} = \hbar v_f (\sigma_x k_y - \sigma_y k_x) + \Delta_h \sigma_z + U \sigma_x \quad (13)$$

The wave functions for the Hamiltonian in Eq. 13 are

$$\Psi_{\eta} = \frac{1}{\sqrt{2}} \begin{pmatrix} \lambda_{\eta}(k) \exp(i\theta) \\ \eta \lambda_{-\eta}(k) \end{pmatrix} \quad (14a)$$

where λ_η is

$$\lambda_\eta = \sqrt{1 \pm \frac{\Delta_h}{\sqrt{(\Delta_h^2 + (\hbar v_f k_y + U)^2 + (\hbar v_f k_x)^2)}}} \quad (14b)$$

and $\theta = \tan^{-1} \frac{k_y}{(k_x + U)}$. The corresponding eigen values are

$$\varepsilon(k) = \sqrt{(\Delta_h^2 + (\hbar v_f k_y + U)^2 + (\hbar v_f k_x)^2)} \quad (15)$$

The scattering time by a direct application of Fermi golden rule in the case of a carrier that tunnels through the band gap open asymmetric thin film, for instance, beginning from a $+k$ state on the top surface and settling in to a $-k$ state on the lower surface (opposite helicity) is

$$\begin{aligned} \frac{1}{\tau} &= \frac{2\pi}{\hbar} g(\varepsilon) V_0^2 \gamma \int_0^\pi \sin^2 \frac{\phi}{2} \cos^2 \frac{\phi}{2} (1 - \cos \phi) d\phi \\ &= \frac{\varepsilon \pi}{4\hbar^3 v_f^2} V_0^2 \gamma \end{aligned} \quad (16)$$

where $\gamma = \frac{((\hbar v_f k_y + U)^2 + (\hbar v_f k_x)^2)}{\Delta^2 + ((\hbar v_f k_y + U)^2 + (\hbar v_f k_x)^2)}$

C. Scattering due to a magnetic impurity

Impurities impregnated on the TI surface which possess a finite magnetic moment break time reversal symmetry (TRS). A broken TRS gives a non-zero expectation value for spin polarization along an axis aligned to the outward normal to the TI surface. To compute the elastic scattering rate in this case, we must re-evaluate the spin suppression factor $\zeta(s, s')$ which was set to $\cos^2 \frac{\phi}{2}$. The spin polarization vectors, bearing in mind the helical structure of the surface states are therefore given by

$$\begin{aligned} \langle S_x \rangle &= \frac{\hbar}{2} \langle \Psi_+ | \begin{pmatrix} 0 & 1 \\ 1 & 0 \end{pmatrix} | \Psi_+ \rangle \\ &= \frac{\hbar v_f k}{\sqrt{\Delta^2 + (\hbar v_f k)^2}} \cos \theta_1 \end{aligned} \quad (17a)$$

$$\begin{aligned} \langle S_y \rangle &= \frac{\hbar}{2} \langle \Psi_+ | \begin{pmatrix} 0 & -i \\ i & 0 \end{pmatrix} | \Psi_+ \rangle \\ &= \frac{\hbar v_f k}{\sqrt{\Delta^2 + (\hbar v_f k)^2}} \sin \theta_1 \end{aligned} \quad (17b)$$

$$\begin{aligned} \langle S_z \rangle &= \frac{\hbar}{2} \langle \Psi_+ | \begin{pmatrix} 1 & 0 \\ 0 & -1 \end{pmatrix} | \Psi_+ \rangle \\ &= \frac{\Delta}{\sqrt{\Delta^2 + (\hbar v_f k)^2}} \end{aligned} \quad (17c)$$

The final spin polarization vector is

$$\mathbf{S} = S_x \hat{i} + S_y \hat{j} + S_z \hat{k} \quad (18)$$

The spin suppression factor between two states $|k(\theta_1), s\rangle$ and $|k'(\theta_2), s'\rangle$ suffering an angular elastic ($|k| = |k'|\rangle$) scattering of $\phi = \theta_1 - \theta_2$ is therefore

$$\begin{aligned} \zeta(s, s') &= \cos^2 \left[\frac{1}{2} \cos^{-1} \frac{s \cdot s'}{|s||s'|} \right] \\ &= \cos^2 \left[\frac{1}{2} \cos^{-1} \frac{\Omega_1^2 \cos \phi + \Omega_2^2}{\Omega_1^2 + \Omega_2^2} \right] \end{aligned} \quad (19a)$$

where

$$\begin{aligned} \Omega_1 &= \frac{\hbar v_f k}{\sqrt{\Delta^2 + (\hbar v_f k)^2}} \\ \Omega_2 &= \frac{\Delta}{\sqrt{\Delta^2 + (\hbar v_f k)^2}} \end{aligned} \quad (19b)$$

The magnetic field induced band gap is $\Delta = \frac{1}{2} g \mu_B B_z$. As before, the scattering time can be computed using Eq. 8; further, in presence of a magnetic field, time reversal symmetry is lost and back scattering is no longer forbidden. Carriers on the surface after scattering can therefore occupy states of opposite helicity or in other words with a reversed k vector (for example, $+k_1$ to $-k_2$, such that $|k_1| = |-k_2|$ for an elastic scattering). The scattering times when the final scattered states have identical ($+k_1$ to $+k_2$ and $|k_1| = |k_2|$) or opposite helicity will be different and can be calculated as follows. We first establish the scattering rate between states of identical helicity.

$$\frac{1}{\tau} = \frac{2\pi}{\hbar} g(\varepsilon) \int_0^\pi d\phi |\langle \Psi_+ | V_0 \zeta(s, s') | \Psi_+ \rangle|^2 (1 - \cos \phi) \quad (20a)$$

Inserting the spin scattering factor using Eq. 19a and wave functions from Eq. 6b and carrying out the straight forward algebra yields

$$\frac{1}{\tau} = \frac{2\varepsilon}{\hbar^3 v_f^2} V_0^2 \int_0^\pi d\phi \cos^2 \vartheta \left\{ \cos^2 \frac{\phi}{2} + \kappa \sin^2 \frac{\phi}{2} \right\} (1 - \cos \phi) \quad (20b)$$

where $\kappa = \frac{\Delta^2}{\Delta^2 + (\hbar v_f k)^2}$. The equation can be numerically evaluated as shown in Sec III. A similar integral for scattering between states of opposite helicity can be written

$$\frac{1}{\tau} = \frac{2\varepsilon}{\hbar^3 v_f^2} V_0^2 \int_0^\pi d\phi \cos^2 \vartheta \left\{ \frac{(\hbar v_f k)^2}{\Delta^2 + (\hbar v_f k)^2} \sin^2 \frac{\phi}{2} \right\} (1 - \cos \phi) \quad (20c)$$

where $\vartheta = \left[\frac{1}{2} \cos^{-1} \frac{\Omega_1^2 \cos \phi + \Omega_2^2}{\Omega_1^2 + \Omega_2^2} \right]$ and Ω_1 and Ω_2 are defined in Eq. 19b.

III. Influence of warping on surface conductivity

Under a weak external force, the deviation of the electron distribution from the thermal equilibrium value can be assumed to be small which allows us to linearize Boltzmann distribution within the relaxation time approximation. The conductivity can therefore be written as

$$\sigma = \frac{e^2 v_f^2}{2} \int dE g(E) \tau \left(-\frac{\partial f}{\partial E} \right) \quad (21)$$

which at $T = 0$ yields $\sigma = \frac{e^2 v_f^2}{2} g(E) \tau$, where we substitute for the diffusion constant D in the original Einstein relation $\sigma = e^2 g(E) D$ as $D = \frac{v_f^2 \tau}{2}$ for a two-dimensional system. The scattering time for each scenario considered can be inserted from their respective expressions derived above. Finally, we note that the expressions derived for scattering time and conductivity undergo a modification if warping terms are explicitly included in the analysis. More precisely, the band gap Δ modifies to $\Delta + \hbar^3 \lambda k^3 \cos 3\theta$ and the density of states also undergoes a change as shown below

$$D(\epsilon)_{warp} = \int \frac{dk}{(2\pi)^2} \delta(\epsilon - E(k)) \quad (22a)$$

$$= \frac{1}{(2\pi)^2} \int_0^{2\pi} d\theta \int_0^\infty k dk \sum_j \frac{\delta(k - k_j)}{|g'(k_j)|} \quad (22b)$$

$$= \frac{1}{(2\pi)^2} \sum_j \int_0^{2\pi} d\theta \frac{k_j}{|g'(k_j)|} \quad (22c)$$

We have used the identity $\delta(g(x)) = \sum_j \frac{\delta(x - x_j)}{|g'(x_j)|}$ such that $g(x_j) = 0$ and there are no multiple zeros. x_j is a simple zero of $g(x)$. The function $g(x)$ takes the form

$$g(x) = \epsilon - \sqrt{\hbar v_f^2 k^2 + \lambda^2 \hbar^6 k^6 \cos^2(3\theta)} \quad (23)$$

The band gap split Δ is ignored since it is swamped by the warping correction at points in momentum space away from the Dirac cones at Γ . The k_j in Eq. 22c are obtained by determining roots of Eq. 23. Expanding Eq. 23 yields

$$\hbar v_f^2 k^2 + \lambda^2 \hbar^6 k^6 \cos^2(3\theta) - \epsilon^2 = 0 \quad (24a)$$

Rearranging, Eq. 24a is written as a cubic equation with k^2 as the variable

$$\lambda^2 \hbar^6 \cos^2(3\theta) (k^2)^3 + \hbar v_f^2 k^2 - \epsilon^2 = 0 \quad (24b)$$

The real solution for k^2 is of the form

$$(\omega_1 + \omega_2)^{1/3} - (|\omega_1 - \omega_2|)^{1/3} \quad (25)$$

where ω_1 and ω_2 are defined as follows

$$\omega_1 = \frac{1}{2} \left(\frac{\epsilon}{\lambda \hbar^3 \cos(3\theta)} \right)^2 \quad (26a)$$

and

$$\omega_2 = \sqrt{\frac{1}{27} \left(\frac{\hbar v_f}{\lambda \hbar^3 \cos(3\theta)} \right)^6 + \frac{1}{4} \left(\frac{\epsilon}{\lambda \hbar^3 \cos(3\theta)} \right)^4} \quad (26b)$$

Finally evaluating the derivative $g'(x)$, we have

$$g'(x) = \mp \frac{\hbar v_f^2 k + 3\lambda^2 \hbar^6 k^5 \cos^2(3\theta)}{\sqrt{\hbar v_f^2 k^2 + \lambda^2 \hbar^6 k^6 \cos^2(3\theta)}} \quad (27)$$

Putting all of them together, the density of states at any given zero of $g(x)$, x_j can be written as

$$D(\epsilon) = \frac{1}{(2\pi)^2} \int_0^{2\pi} d\theta k \frac{\sqrt{(\hbar v_f)^2 k^2 + \lambda^2 \hbar^6 k^6 \cos^2(3\theta)}}{(\hbar v_f)^2 k + 3\lambda^2 \hbar^6 k^5 \cos^2(3\theta)} \quad (28a)$$

Simplifying, we get

$$D(\epsilon) = \frac{1}{(2\pi)^2} \int_0^{2\pi} d\theta k \frac{\epsilon}{(\hbar v_f)^2 k + 3\lambda^2 \hbar^6 k^5 \cos^2(3\theta)} \quad (28b)$$

Noting that energy ϵ is a constant, the final form for $D(\epsilon)$ is

$$D(\epsilon) = \frac{\epsilon}{(2\pi)^2} \int_0^{2\pi} d\theta \frac{k^2}{\epsilon^2 + 2\lambda^2 \hbar^6 k^6 \cos^2(3\theta)} \quad (28c)$$

In simplifying the above expression, we have used the Dirac cone energy expression $\sqrt{\hbar v_f^2 k^2 + \lambda^2 \hbar^6 k^6 \cos^2(3\theta)}$. Inserting for k from Eq. 25, 26a, and 26b, the final expression for density of states (Eq. 28c) is evaluated numerically in Section IV.

IV. Results

All results derived in this paper use the two-band model (Eq. 2) which employs phenomenological parameters to describe band gap splitting and inter-surface coupling in case of an asymmetric thin film. These parameters can be directly established from a first-principles calculation^{19,20} or obtained, as done here, by numerically diagonalizing the four-band Hamiltonian of Eq. 1. The required parameters are read off the dispersion plot. The Fermi velocity of the surface states is taken as 5×10^5 m/s for all calculations shown.

A. Non-magnetic impurities

We first plot the dispersion relationships (Fig. 1) for a nine and three quintuple layer Bi_2Se_3 topological insulator film. Each quintuple layer is about 1.0 nm. The three quintuple layer film has its top and bottom surfaces coupled (hybridized surfaces) which induces a finite band gap. On the surface of a 9.0 nm thick Bi_2Se_3 topological insulator slab which has zero-gap states, a uniform, dilute, and non-interacting spherical impurity scattering potential of 10.0 meV is assumed to be present. Electrons scatter from such fixed impurities with no internal

excitations elastically. The scattering time is computed at an energy equal to the Fermi level which is set to 100.0 meV. At this energy, the density of states (DOS), using Eq. 3a is $2.93 \times 10^{-6} \text{meV}^{-1} \text{\AA}^{-2}$. Inserting the DOS in the scattering time equation (Eq. 9) yields a value equal to 9.076×10^{-10} seconds. It is important to note that the Fermi-level can be raised up to 0.2 eV, beyond which we reach the bulk conduction bands of Bi_2Se_3 . The bulk conduction bands of the slab can be seen to begin from the 0.2 eV mark in Fig. 1.

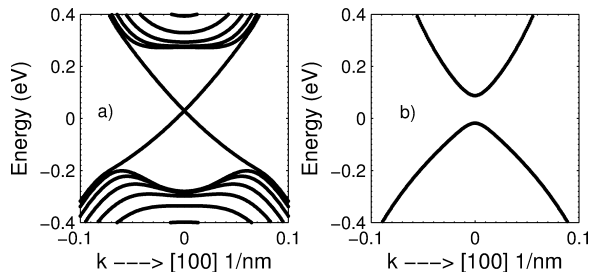


FIG. 1: Dispersion of a 9.0 nm thick Bi_2Se_3 topological insulator slab around the Dirac point (Fig. 1a) at 0.02 eV. The dispersion of the thin film (3.0 nm thick) (Fig. 1b) shows two Dirac hyperbolas when the surface states hybridize.

For the case of a thin TI film, the possibility of an electron tunneling through the bulk and reaching a state of opposite helicity on the second surface must be accounted for. The variation in band gap of the surface states for a thin film with varying thickness is plotted in Fig. 2. Retaining the parameters from the case of scattering between states of identical helicity and setting the band gap Δ in Eq. 12 to 100.0 meV, the corresponding scattering time is determined to be 8.309×10^{-10} seconds. The scattering time is similar to the one obtained when scattered carriers are constrained only to occupy another state of identical helicity on the same surface. It is easy to see from Eq. 9 and Eq. 12 that the ratio of scattering times between the two cases is $\frac{(\hbar v_f k)^2}{\Delta^2 + (\hbar v_f k)^2}$. The ratio is significant when k is close to the Γ point or the Dirac cone but tends to unity at larger k values since the hybridization induced band gap split is generally a small number. As pointed out later, at points far away from Γ where the Dirac crossing happens, the density of states using Eq. 3b is inadequate.

We next turn our attention to a TI thin film grown on a substrate that renders the structure asymmetric by creating a spatially-dependent dipole moment. A simple way to mimic the effect of a substrate is to model the film with two different surface terminations as depicted in Fig. 3. The asymmetric potential gives structural inversion asymmetry (SIA) which means that the two surfaces do not have equi-energetic Dirac cones. As shown in Fig. 4, a TI film with bismuth and tellurium surface termination possesses a non-zero dipole moment^{21–23} with an oscillating charge pattern in bulk of the film. In

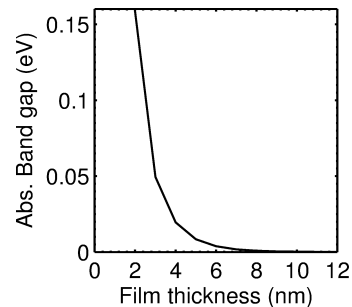


FIG. 2: Band-gap opening as a function of Bi_2Se_3 film thickness. A band gap opens because the wave function from the two surfaces penetrate the bulk and hybridize.

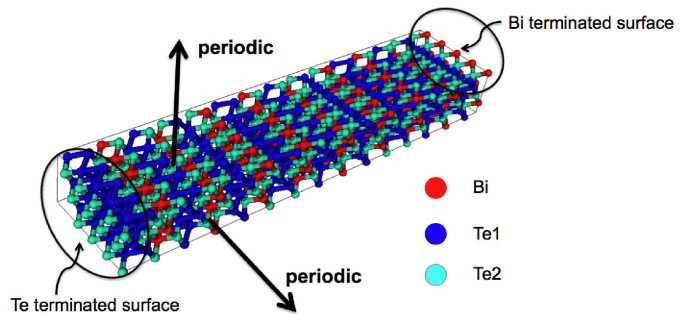


FIG. 3: A 9.0 nm thick Bi_2Te_3 ultra-thin body oriented along the x-axis. The two surfaces have Bi and Te termination thus making them chemically non-equivalent.

absence of the SIA potential, the surface states consist of spin degenerate conduction and valence bands²⁴ separated by the hybridization gap Δ while the substrate induced asymmetry leads to a Rashba splitting.²⁵ The actual band gap (Eq. 15) varies with the overall dipole moment. For the thin film considered here, U is found to be 1.0 eV²¹ and using identical parameters as before, the scattering time is 9.025×10^{-10} seconds. In evaluating the scattering time, the wave vector is assumed to only have a k_x component equal to 0.1 $1/\text{\AA}$.

The scattering time in all the three cases is roughly the same which suggests that the band gap opening and the dipole moment do not significantly affect the results since the factors $\frac{(\hbar v_f k)^2}{\Delta^2 + (\hbar v_f k)^2}$ and

$$\frac{\left((\hbar v_f k_y + U)^2 + (\hbar v_f k_x)^2 \right)}{\Delta^2 + \left((\hbar v_f k_y + U)^2 + (\hbar v_f k_x)^2 \right)}$$

from Eq. 12 and Eq. 16 at moderate k vectors are numerically close. These factors, nonetheless, have a relatively important contribution when the ratio of band splitting energy (Δ) to the Fermi-energy $\hbar v_f k$ is not negligible which is possible for very small values of the momentum vector.

All the scattering times discussed here include the spin suppression factor whose contribution can be gauged by evaluating the scattering rate equation for a zero-gap TI

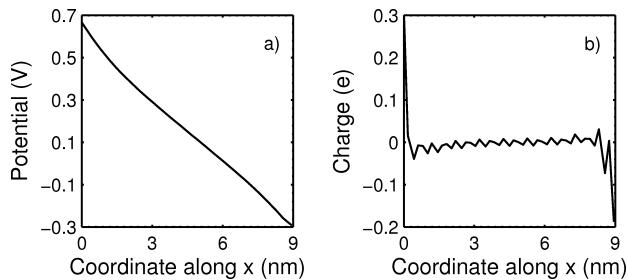


FIG. 4: The spatially-dependent electrostatic potential (Fig. 4a) and charge on each atomic node is plotted against the x coordinate of the Bi_2Te_3 thin film. This thin-film has Bi and Te termination on the surfaces. An oscillating charge pattern (Fig. 4b) is obtained for non-equivalent surface termination.

with impurities (Eq. 9) without the $\cos^2\frac{\phi}{2}$ term. Such a calculation gives a scattering time of 2.8×10^{-10} seconds, which is a reduction by a factor of 3.24. A shorter scattering time signifies lower mobility and conductivity²⁶ which can be easily explained by noting that the high mobility of surface states is attributed to spin-protected forbidden back scattering. The condition to forbid back scattering is relaxed by ignoring the spin-suppression factor of $\cos^2\frac{\phi}{2}$. We also note, as shown in Ref. 27, the scattering time in a gapped topological insulator (trivial case) is four-fold higher compared to a zero-gapped topological insulator (non-trivial case). The factor of 3.24 in the present case where the suppression factor controls back scattering matches well with the previously derived result. In passing we mention here, that the dipole moment, in principle, at a critical value, can close the band gap and re-open as an instance of topological phase transition.²⁸

B. Magnetic impurities and warped bands

The helical nature^{29,30} of the surface states of a pristine topological insulator ensures that there is a definite in-plane spin polarization. Magnetic impurities on the surface give an additional out-of-plane spin component³¹ thus essentially turning the spin-polarization to a three-dimensional vector. Scattering times corresponding to a 9.0 nm and 3.0 nm thin film are presented for discussion. For the 3.0 nm thin film, we consider the case of a carrier tunneling to the other surface and occupying a state of opposite helicity. Proceeding along same lines as for non-magnetic impurities with the spin suppression factor now modified such that spins are aligned to the effective spin-polarization vector, yields scattering times equal to 7.530×10^{-10} seconds and 6.935×10^{-10} seconds for the 9.0 nm and 3.0 nm TI films respectively. As a first check, the scattering times are shorter than 9.076×10^{-10} seconds, which is the corresponding result for a zero-gap topological insulator film. The presence of a band gap reduces the scattering time, augments the large angle scattering

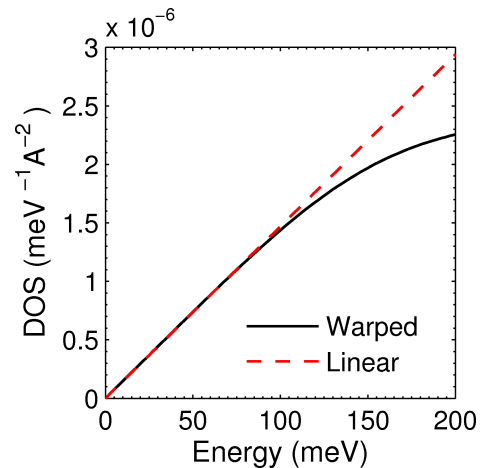


FIG. 5: The density of states for a warped dispersion deviates from the expression obtained for linear bands at higher energies. At higher energies, the warping terms significantly contribute to the overall energy spectrum of the TI surface states. The warping strength in this calculation was set to $500.0 \text{ eV}\text{\AA}^{-3}$.

and consequently lowers the mobility as expected. In calculations shown here, we have explicitly neglected the orbital coupling of the magnetic field through a Peierls substitution and retained only the spin coupling through the Zeeman term. The Zeeman term can be attributed to an externally applied magnetic field or the exchange field of a ferromagnet layered on the surface of a TI.³²

At this point, it is worthwhile to establish the change in scattering rates due to warped nature of bands, if the momentum vectors are not in the immediate proximity of the Γ point. The warped bands modify the density of states as derived in Eq. 28c. A comparative plot of density of states obtained from a linear dispersion and with warping terms included is shown in Fig. 5. The density of states for the warped case was determined by numerically integrating Eq. 28c.

The scattering time for a carrier described by a warped Hamiltonian (Eq. 4) on surface of a zero-gap topological insulator whose initial and final states are of same helicity is 1.541×10^{-9} seconds. The scattering time is higher compared to 7.530×10^{-10} seconds because of a lower density of states with warped bands. It is well-known from semi-classical transport theory³³ that a lower density of states reduces scattering and increases mobility. Scattering times for a range of band gaps for the linear and warped dispersion models is shown in Fig. 6. The scattering time decreases almost linearly under higher magnetic fields (increased band gaps) for both the Dirac and warped dispersion which is indicative of a greater magnetoresistance. The origin of the enhanced magnetoresistance is through a large angle scattering ($1 - \cos\theta$) term that enters the analysis in the scattering rate equation. Further, since the electric conductivity, as evident from Eq. 21, is directly proportional to the scattering time, the warped model would yield a higher value. In other words,

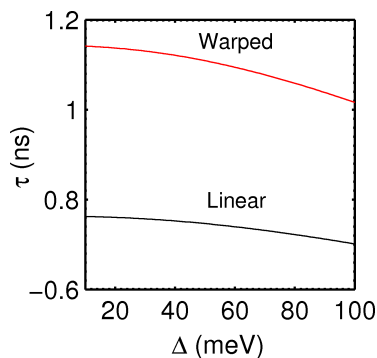


FIG. 6: The scattering time on surface of a magnetically gapped topological insulator is higher for the warped band model (warping strength = $500.0 \text{ eV}\text{\AA}^{-3}$) because of a lower density of states. The scattering time also decreases with a greater magnetic field induced band gap indicating lower mobility or a higher magnetoresistance.

electric conductivity is an implicit function of momentum space; at k points away from Γ , the warped Hamiltonian which is a better description of electronic spectrum of surface states yields lower density of states and a higher electron velocity.

V. Surface conductivity and mean free path

The conductivity on the impure surface of a topological insulator can be estimated by a direct application of Eq. 21. We consider a non-magnetic impurity of density $n_i = 0.5 \times 10^{10}$. The scattering potential is 500.0 eV . The scattering event takes place at a Fermi level set to 200.0 meV for which the density of states (using Eq. 3a for linear bands) is $5.877 \times 10^{-6} \text{ meV}^{-1} \text{ \AA}^{-2}$. The scattering time for this case turns out to be 9.076×10^{-14} seconds. Putting all these numbers in Eq. 21, the surface conductivity, expressed in terms of the quantum conductance $\sigma = \frac{2e^2}{h}$ is 137.595σ . The conductivity at large k values is reduced since the corresponding density of states must now be computed with warped bands. The DOS with warped bands at 200.0 meV evaluates to (by numerical integration of Eq. 28c) $4.51 \times 10^{-6} \text{ meV}^{-1} \text{ \AA}^{-2}$ while the scattering time is 1.183×10^{-13} seconds. The surface conductivity value of 137.721σ is only marginally higher than the corresponding 137.595σ for linear bands. Another useful that can be easily computed is the mean free path given as $v_f\tau$. The numbers for linear and warped bands are 45.38 nm and 59.15 nm respectively.

While the above analysis does not account for scatter-

ing events which involve phonons and charged impurities, the mean free paths obtained suggest that transport in a topological insulator channel material for a conventional field-effect transistor in a miniaturized device will be ballistic. The experimentally determined mean free path in GaAs, a high-mobility semiconductor, is approximately 34.0 nm at room temperature.

VI. Conclusion

In this work we have theoretically presented the evaluation of scattering times on the surface of a 3D topological insulator using Boltzmann transport. The role of spin suppression factor which comes from the topological nature of the states and explains the higher mobility on a TI surface is highlighted. It is found that in case of a magnetically split TI surface, the alignment of the spin polarization vectors to the effective magnetic field reduces the overall scattering time. The influence of density of states from a warped model is analyzed and a higher mobility and electric conductivity value is established. The enhancement is attributed to the reduced density of states. In carrying out these calculations we have assumed a uniform Fermi velocity for the surface states though that may not be true for all materials that exhibit topological insulator behaviour. In particular, the topological Kondo insulator^{34,35} which has Fermi pockets³⁶ with varying velocities is a case in point. Also, in a more careful calculation, which could be potential future work, preferential scattering directions dependent on the underlying crystal symmetry must be considered. Finally, we note that because of the helical structure of the surface state, the spin polarization vector must have a definite polarization for a given k state. It is tacitly assumed that the spin relaxation happens at a much faster rate than momentum relaxation; in case the spin-relaxation time, through the well-known Dyakanov-Perel or Elliot-Yafet relaxation mechanisms^{37,38} is comparable to the momentum relaxation time, the overall scattering rate and mobility will be altered. This aspect has not been investigated here.

Acknowledgments

This work at Boston University was supported in part by the BU Photonics Center and U. S. Army Research Laboratory through the Collaborative Research Alliance (CRA) for MultiScale multidisciplinary Modeling of Electronic materials (MSME). PS also thanks Saumitra Mehrotra of Freescale Semiconductors for reading the manuscript.

* Electronic address: parijats@bu.edu

¹ X.-L. Qi and S.-C. Zhang, Reviews of Modern Physics **83**, 1057 (2011).

² C.-X. Liu, H. Zhang, B. Yan, X.-L. Qi, T. Frauenheim, X. Dai, Z. Fang, and S.-C. Zhang, Physical review B **81**,

041307 (2010).

³ P. Roushan, J. Seo, C. V. Parker, Y. Hor, D. Hsieh, D. Qian, A. Richardella, M. Z. Hasan, R. Cava, and A. Yazdani, Nature **460**, 1106 (2009).

⁴ X. Zhou, C. Fang, W.-F. Tsai, and J. Hu, Physical Review

- B **80**, 245317 (2009).
- ⁵ G. Yin, D. Wickramaratne, Y. Zhao, and R. K. Lake, Applied Physics Letters **105**, 033118 (2014).
 - ⁶ W.-Y. Shan, H.-Z. Lu, and S.-Q. Shen, New Journal of Physics **12**, 043048 (2010).
 - ⁷ L. Bao, L. He, N. Meyer, X. Kou, P. Zhang, Z.-g. Chen, A. V. Fedorov, J. Zou, T. M. Riedemann, T. A. Lograsso, et al., Scientific reports **2** (2012).
 - ⁸ Y. S. Kim, M. Brahlek, N. Bansal, E. Edrey, G. A. Kapilevich, K. Iida, M. Tanimura, Y. Horibe, S.-W. Cheong, and S. Oh, Physical Review B **84**, 073109 (2011).
 - ⁹ S.-Y. Xu, Y. Xia, L. Wray, S. Jia, F. Meier, J. Dil, J. Osterwalder, B. Slomski, A. Bansil, H. Lin, et al., Science **332**, 560 (2011).
 - ¹⁰ C.-X. Liu, X.-L. Qi, H. Zhang, X. Dai, Z. Fang, and S.-C. Zhang, Physical Review B **82**, 045122 (2010).
 - ¹¹ H. Zhang, C.-X. Liu, X.-L. Qi, X. Dai, Z. Fang, and S.-C. Zhang, Nature physics **5**, 438 (2009).
 - ¹² Z. Alpichshev, J. Analytis, J.-H. Chu, I. R. Fisher, Y. Chen, Z.-X. Shen, A. Fang, and A. Kapitulnik, Physical review letters **104**, 016401 (2010).
 - ¹³ S. Souma, K. Kosaka, T. Sato, M. Komatsu, A. Takayama, T. Takahashi, M. Kriener, K. Segawa, and Y. Ando, Physical review letters **106**, 216803 (2011).
 - ¹⁴ Y. Wang, D. Hsieh, D. Pilon, L. Fu, D. Gardner, Y. Lee, and N. Gedik, Physical review letters **107**, 207602 (2011).
 - ¹⁵ L. Fu, Physical review letters **103**, 266801 (2009).
 - ¹⁶ S. Basak, H. Lin, L. Wray, S.-Y. Xu, L. Fu, M. Hasan, and A. Bansil, Physical Review B **84**, 121401 (2011).
 - ¹⁷ G. D. Mahan, *Many-particle physics* (Springer Science & Business Media, 2000).
 - ¹⁸ F. Han, *A modern course in the quantum theory of solids* (World Scientific, 2013).
 - ¹⁹ W. Zhang, R. Yu, H.-J. Zhang, X. Dai, and Z. Fang, New Journal of Physics **12**, 065013 (2010).
 - ²⁰ K. Park, C. De Beule, and B. Partoens, New Journal of Physics **15**, 113031 (2013).
 - ²¹ P. Sengupta, Ph.D. thesis, Purdue University (2013).
 - ²² This figure was produced using the NEMO5 nano-electronics simulator; more information can be found at <https://engineering.purdue.edu/gekcogrp/software-projects/nemo5/>. See Ref. 23 for a description of the simulator.
 - ²³ J. E. Fonseca, T. Kubis, M. Povolotskyi, B. Novakovic, A. Ajoy, G. Hegde, H. Ilatikhameneh, Z. Jiang, P. Sengupta, Y. Tan, et al., Journal of Computational Electronics **12**, 592 (2013).
 - ²⁴ P. Sengupta, T. Kubis, Y. Tan, and G. Klimeck, Journal of Applied Physics **117**, 044304 (2015).
 - ²⁵ Y. S. Dedkov, M. Fomin, U. Rüdiger, and C. Laubschat, Physical review letters **100**, 107602 (2008).
 - ²⁶ D. K. Ferry, S. M. Goodnick, and J. Bird, *Transport in nanostructures*, vol. 6 (Cambridge University Press, 2009).
 - ²⁷ P. Sengupta, G. Klimeck, et al., arXiv preprint arXiv:1503.06224 (2015).
 - ²⁸ H. Li, L. Sheng, D. Sheng, and D. Xing, Physical Review B **82**, 165104 (2010).
 - ²⁹ O. V. Yazyev, J. E. Moore, and S. G. Louie, Physical review letters **105**, 266806 (2010).
 - ³⁰ L. A. Wray, S.-Y. Xu, Y. Xia, D. Hsieh, A. V. Fedorov, Y. San Hor, R. J. Cava, A. Bansil, H. Lin, and M. Z. Hasan, Nature Physics **7**, 32 (2011).
 - ³¹ Q. Liu, C.-X. Liu, C. Xu, X.-L. Qi, and S.-C. Zhang, Physical review letters **102**, 156603 (2009).
 - ³² D. Zhang, A. Richardella, D. W. Rench, S.-Y. Xu, A. Kandala, T. C. Flanagan, H. Beidenkopf, A. L. Yeats, B. B. Buckley, P. V. Klimov, et al., Physical Review B **86**, 205127 (2012).
 - ³³ J. M. Ziman, *Principles of the Theory of Solids* (Cambridge university press, 1972).
 - ³⁴ M. Neupane, N. Alidoust, S. Xu, T. Kondo, Y. Ishida, D.-J. Kim, C. Liu, I. Belopolski, Y. Jo, T.-R. Chang, et al., Nature communications **4** (2013).
 - ³⁵ M. Dzero, K. Sun, P. Coleman, and V. Galitski, Physical Review B **85**, 045130 (2012).
 - ³⁶ Z.-H. Zhu, A. Nicolaou, G. Levy, N. Butch, P. Syers, X. Wang, J. Paglione, G. Sawatzky, I. Elfmov, and A. Damascelli, Physical review letters **111**, 216402 (2013).
 - ³⁷ D. Huertas-Hernando, F. Guinea, and A. Brataas, Physical review letters **103**, 146801 (2009).
 - ³⁸ M. I. Dyakonov, *Spin physics in semiconductors*, vol. 157 (Springer Science & Business Media, 2008).